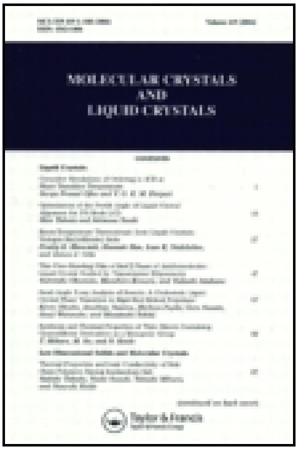

Molecular Crystals and Liquid Crystals

Publication details, including instructions for authors and subscription information:
http://www.tandfonline.com/loi/gmcl20

Formation and Characterization of Gold and Silver Nanoparticles on Silica Nanospheres

P.-T. Miclea [a] & H. Hofmeister [b]

[a] Department of Electrical and Information Engineering, Institute of Materials Science, Wuppertal, Germany

[b] Max Planck Institute of Microstructure Physics, Halle (Saale), Germany

Version of record first published: 18 Oct 2010

To cite this article: P.-T. Miclea & H. Hofmeister (2004): Formation and Characterization of Gold and Silver Nanoparticles on Silica Nanospheres, Molecular Crystals and Liquid Crystals, 417:1, 135-147

To link to this article: http://dx.doi.org/10.1080/15421400490478579

Mol. Cryst. Liq. Cryst., Vol. 417, pp. 135/[619]–147/[631], 2004
Copyright © Taylor & Francis Inc.
ISSN: 1542-1406 print/1563-5287 online
DOI: 10.1080/15421400490478579

FORMATION AND CHARACTERIZATION OF GOLD AND SILVER NANOPARTICLES ON SILICA NANOSPHERES

P.-T. Miclea
Institute of Materials Science, Department of Electrical and Information Engineering, University of Wuppertal, Wuppertal, D-42097, Germany

H. Hofmeister
Max Planck Institute of Microstructure Physics, Halle (Saale), D-06120, Germany

Novel optical effects are expected by appropriately arranging metal nanoparticles on the surface of spherical insulating materials. Optical resonances of this nanostructures from near infrared to the visible range may be tuned by adjusting the oxide size, size of the metal particles and the filling factor. For a better control of the optical properties of such composite materials the best choice as oxide material is the monodisperse oxide particles. Water-soluble metal precursor complexes hydrogentetrachloroaurate and silver acetate have been employed. The optical properties of these materials correspond to their overall structure of nanoparticulate composites having a very low filling factor of the metal phase.

INTRODUCTION

Small metal particles exhibit in the visible range optical properties different from those of the bulk material due to their size and shape [1]. At the beginning of the last century the study of color changes of various types of glasses [2,3] triggered this research area. Moreover, another area of interest was to find new materials with a dielectric function different from that of the bulk material that firstly were applied to improve photovoltaic conversion [4,5]. In order to study the properties of nanoparticles on oxide surfaces from the optical point of view in this work the Mie theory and also

Address correspondence to P.-T Miclea, Institute of Materials Science, Department of Electrical and Information Engineering, University of Wuppertal, Wuppertal, D-42097, Germany. E-mail: miclea@uni-wuppertal.de

the Maxwell-Garnet theory are applied for the case of small filling factor, and the Bruggeman model for higher values.

From the extinction cross section and knowledge of the filling factor f and the volume of one particle v_0, it is straightforward to calculate the extinction coefficient of the sample $\alpha_{\mathrm{ext}} = f\sigma_{\mathrm{ext}}/v_0$. Spherical metal particles with sizes less than 10 nm have a dielectric function $\varepsilon = \varepsilon' + i\varepsilon''$ in the dipolar approximation and the extinction coefficient can be written as:

$$\alpha_{ext} = 18\pi\frac{fv_0\varepsilon_m^{3/2}}{\lambda}\frac{\varepsilon''}{\left[(\varepsilon' + \varepsilon_m)^2 + \varepsilon''^2\right]} \tag{1}$$

where the real and imaginary part of the dielectric function are described using the simple Drude model and ε_m is the real part of the host matrix dielectric function. If metal particles form a shell around a dielectric host material (core-shell structures) in dipolar approximation for a core with one shell the absorption cross section can be calculated using:

$$\sigma_{abs} = 18\pi\frac{V\varepsilon_m^{3/2}}{\lambda}\mathrm{Im}\left\{\frac{(\varepsilon - \varepsilon_m)(\varepsilon_c + 2\varepsilon) + g(\varepsilon_c - \varepsilon)(\varepsilon_m + 2\varepsilon)}{(\varepsilon + 2\varepsilon_m)(\varepsilon_c + 2\varepsilon) - g(\varepsilon_c - \varepsilon)(2\varepsilon_m - 2\varepsilon)}\right\} \tag{2}$$

where Im is the imaginary part, ε is the complex dielectric function of the shell, ε_m is the real dielectric function of the host medium, ε_c is the real dielectric function of the core material, V is the volume of the coated sphere and $g = [R/(R+d)]^3$, with R the radius of the core particle, and d the thickness of the shell.

EXPERIMENTAL

Nanoparticle composite materials were investigated from the morphological and structural point of view using electron microscopy. Morphological properties of the samples are studied using transmission electron microscopy (TEM) and the structural characterization of nanoparticles is performed with high resolution electron microscopy (HREM). The optical properties of the nanoparticulate composite materials were investigated by using optical spectroscopy in the visible region. The optical properties of metal particles are deduced from the measurement of the transmittance defined as the ratio between the transmitted and incident light intensity $T = I/I_0$. The Lambert-Beer law gives the extinction coefficient as:

$$\sigma_{ext} = -\ln T \tag{3}$$

The calculation of extinction spectra using the Mie theory for nanoparticles embedded in a dielectric matrix and the extension of this theory for

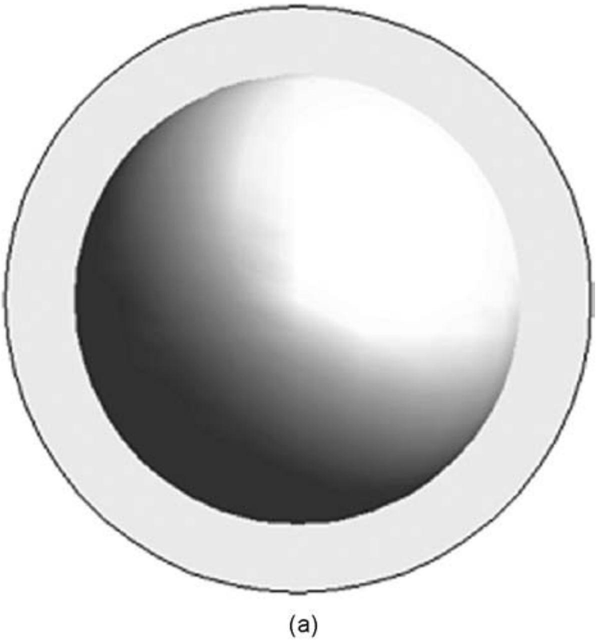

FIGURE 1 Metal nanoparticle formation on silica nanospheres by incipient wetness impregnation (a) and (b), followed by metal precursor reduction upon drying at moderate temperatures (c).

core-shell structures is based on a program described by Kreibig [1] for dipolar approximation and one by Bohren [3] for multipolar approximation. The program for multipolar approximation solves the Bessel-Ricatti functions using backward recurrence. To achieve a better performance the limitations for the order of the calculated Bessel-Ricatti functions are changed using the size parameters proposed by Wiscombe [6].

Potential application as sensors or optical devices governed by novel physical properties requires monodisperse nanospheres. We explored the characteristics of two different classes of such oxide materials. The first one concerns silica nanospheres in the form of powder. A few have been commercially available like Monospher^{TM} 100 with a mean size $\bar{d} = 94.5 \pm 11.4\,\text{nm}$ and Monospher^{TM} 250 with $\bar{d} = 215 \pm 30.5\,\text{nm}$ produced by Merck KgaA. For more flexibility with respect to the size we used monodisperse silica nanospheres synthesized by the Stöber route [7]. This method uses tetraethoxysilane, (TEOS = $Si(OC_2H_5)_4$) as starting material and ethanol as solvent. The reaction takes place in the presence of water and ammonia is used as catalysts to initiate hydrolysis and condensation.

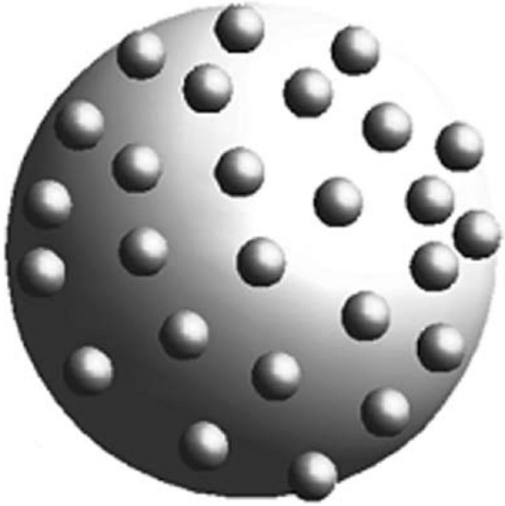

(b)

FIGURE 1 Continued.

The mean size of the silica nanospheres can be very well controlled by the molar concentration of TEOS, water and ammonia.

With the availability of these starting materials a better defined exploration of appropriate coating conditions was possible. The investigations

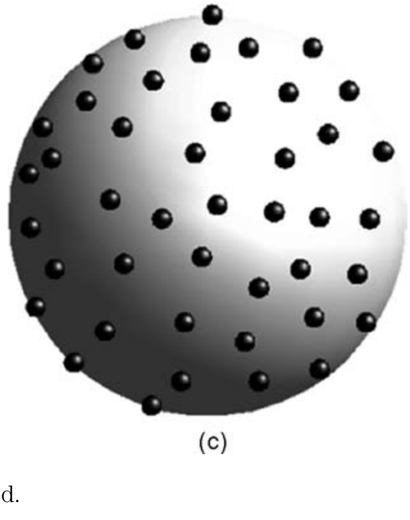

(c)

FIGURE 1 Continued.

have been directed to the metals that exhibit strong surface plasmon resonance effects like Ag and Au. In order to produce spectroscoppically clear (no adhesives!) and photochemically stable (no ligands!) metal nanoparticles deposits the incipient wetness impregnation method, requiring only modest chemical laboratory technique and commercially available chemicals, was successfully applied.

This method, widely used for the preparation of heterogeneous catalysts, consists of wetting a non-planar (powder) substrate by a metal salt solution of certain concentration so as to cover its surface in a defined manner. In catalyst preparation, after drying the impregnated carrier powder, usually a calcination treatment, e.g., in flowing air, is performed resulting in a transformation of the deposited metal salt into an oxide or hydroxide of the metal, that may be reduced, e.g., in flowing hydrogen, in a subsequent reduction step. Since calcination and reduction are usually carried out in a temperature range of about 300 to 800°C, these procedures are not useful for the purpose of metal particle formation under moderate conditions. Instead, we tested if the formation of metal particles could be achieved by simply drying the impregnated silica nanospheres at temperatures below 100°C or even at room temperature. This treatment proved to be successful. The whole procedure is schematically represented in Figure 1 where (a) illustrates the impregnation step, (b) shows the situation after solvent removal, and (c) that upon metal particle formation. The latter step is considered to be sensitively depending on the configuration of terminating groups on the silica surface, since such surface groups obviously provide the reducing radicals required for the reduction of metal ions. Terminating OH- groups usually formed on the oxide surface by dissociative adsorption of water molecules can acquire such properties, depending on their coordination symmetry [8]. Accordingly, metal ion reduction could proceed via the reaction:

$$\equiv Si - OH + M^0 \equiv Si - O\bullet + H^+ + M^0$$

while with $Si{-}O^-$ groups formed by dissociation of hydrogen from the surface hydroxyl the following reaction is possible

$$2 \equiv Si - O^- + 2M^+ \equiv Si - O - Si \equiv +2M^0 + \frac{1}{2}O_2 \uparrow$$

The efficiency of these surface-mediated reduction processes is observed to vary with aging of the silica nanospheres.

The above described metal deposition processes have been applied to monodisperse silica nanospheres, received from Merck with 100 and 250 nm nominal size or laboratory-made by the Stöber method, with sizes in the range of 100 to 300 nm. As metal precursors the water-soluble complexes hydrogentetrachloroaurate $HAuCl_4$ and silvernitrate $AgNO_3$ obtained from Alfa as well as silver acetate $AgOOCCH_3$ from Fluka have been employed. Silica nanospheres and metal complexes were used without further pretreatment. For a certain, precisely measured mass of the oxide, typically 2 g, the mass of metal salt is calculated that is required to achieve a certain metal concentration. This quantity of the metal complex is dissolved in a defined volume of distilled water required to meet the condition of incipient wetness. The solution is added then to the oxide powder and stirred until a uniform color of the sample was observed. Before any further treatment they were stored at room temperature in air for 2 hours. For thermal decomposition of the metal complexes the samples were filled in quartz boats and placed in a quartz tube of 20 mm diameter inside a temperature controlled cylindrical oven. This quartz tube could be evacuated by a membrane pump to a vacuum of about 20 mbar. Since the metal precursors applied are sensitive even to visible light, the above procedure was carried out under dark-room conditions.

The coating of oxide nanospheres by metal nanoparticles aimed at forming core-shell-like structures can be characterized by two parameters, the mean particle size and the coverage, i.e. the portion of the nanosphere surface covered by metal particles. The parameters like origin, age and size of the oxide nanospheres, type and concentration of the precursor complexes may affect the shape of the particle size distribution and the uniformity of the particle arrangement. For the success of efforts to fabricate core-shell structures it is required to adjust the conditions of synthesis so as to avoid bimodal size distributions and particle aggregates which indicate the presence of obstructing inhomogeneities.

Figure 2 shows a characteristic TEM image of Monospher^{TM} silica nanospheres coated by Ag nanoparticles from a 2% silver acetate impregnation upon 2 h drying at 70°C (a) , together with the corresponding size distribution (b). Both representations prove that the deposition method applied results in coverage of the oxide spheres by uniformly arranged very small metal particles of rather narrow size variation. In addition, more or less as by-product, there are some larger particles present that indicate that besides particle formation by nucleation and growth also coalescence and mobility of larger particles must be considered. A closer view on the achieved Ag nanoparticle coating is given by the HREM images. Figure 3 illustrates that (i) the Ag particles are mostly single crystalline in this early stage of growth, (ii) they are facetted by crystallographic low index planes, and (iii) they do not exhibit any truncation owing to substrate-deposit interaction.

All samples with Au nanoparticles have been prepared by employing hydrogentetrachloroaurate as metal precursor either on Monospher^{TM}

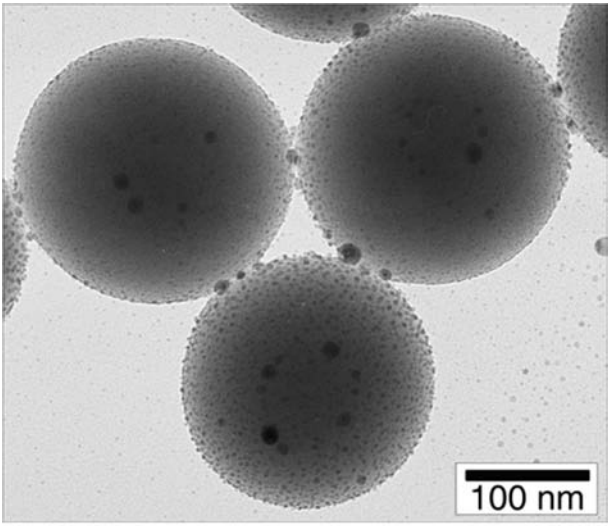

(a)

FIGURE 2 TEM image (a) and size distribution (b) of Ag nanoparticles (2% silver acetate) on Monospher^{TM} silica upon drying 2 h at 70°C.

silica or on Stöber silica (300 nm) nanospheres. Figure 4(a) shows a characteristic HREM image together with the corresponding size distribution of silica coated by Au particles from a 1% precursor sample upon 2 h drying at 70°C. Similar to the experiments with Ag, a dense coverage of uniformly arranged small gold particles of narrow size distribution given in Figure 4(b) is obtained. Accordingly, the crystalline nature and random orientation with respect to each other is ascertained. The tendency to form particles of nearly spherical shape without truncations at the interface is well established owing to the weak interaction between gold deposit and silica substrate that is assumed to be even smaller as in the case of silver. Actually, the particles exhibit cuboctahedral shape rather than that of ideal spheres.

The extinction spectrum of this Ag sample shown in Figure 5 (solid line) does not exhibit a signature of metal particle resonances, but a rather broad extinction in the corresponding region. For comparison, a spectrum calculated for Ag particles in a silica matrix using the Mie theory is shown in the figure (dashed line). The calculation is based on the dipolar approximation for particles of 2 to 2.5 nm size taking into account the quantum size effect expected for this size range. For the real dielectric function of silica a constant value of 2.25 is used and a filling factor of 0.2 is chosen for the Ag component. This results in a reasonable

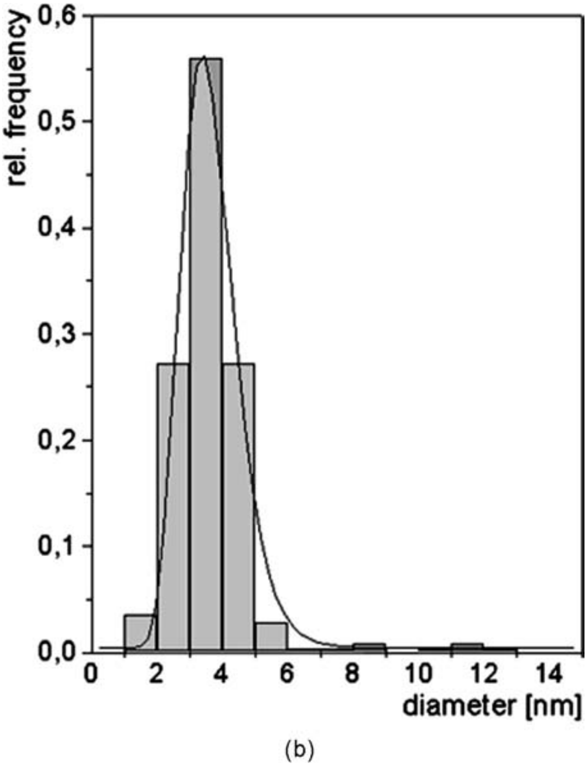

FIGURE 2 Continued.

intensity of the resonance peak with maximum at 425 nm in agreement with the findings of Kreibig [1]. However, the filling factor exceeds by far that corresponding to the silica nanospheres coated by an incomplete layer of Ag nanoparticles. Here, from 215 nm mean diameter of silica spheres and 2.5 nm mean diameter of Ag particles a nominal loading factor (comparable to a filling factor) of 0.0065 is estimated taking into account 19% coverage of the silica surface. Consequently, the spectra of such samples are necessarily dominated by the scattering contributions of silica nanospheres.

Similar as in the case of silver, also with gold there is no indication of nanoparticle surface plasmon resonances at low metal loading and very small particle sizes. The spectrum of the 1% sample dried 2 h at 120°C does only exhibit a rather broad extinction dominated by scattering contributions of silica nanospheres. In contrast to silver, the maximum of the surface plasmon resonance of small gold particles is situated around

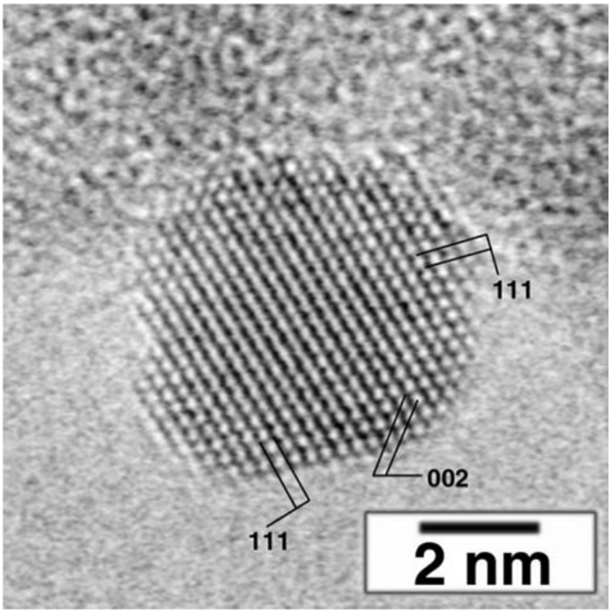

FIGURE 3 HREM image of Ag nanoparticle. The lattice fringes of {111} and {200} types are shown.

550 nm such that it is not completely covered by the extinction of silica nanospheres. Hence, with the occurrence of a sufficient number of particles larger than about 10 nm the resonance damping is less effective and the evolution of metal particle resonances is observed. This behaviour may be demonstrated by the extinction spectra shown in Figure 6 of the samples subjected to additional drying at elevated temperatures. Simultaneously, the color appearance of the sample powder changes from a cloudy yellow to a speckled violet. The apparent blue-shift of the Au particles resonance position from about 565 to 540 nm, seen in the spectra of the additionally dried samples, is not indicative of certain size effects, but most probably due to superposition with the predominating extinction of silica nanospheres. The more the metal plasmon resonance evolves out of the background, the more the maximum of the corresponding shoulder moves towards the true resonance position. Similar results were obtained with the sample prepared by employing 1% metal precursor on Stöber silica (300 nm) upon 2 h drying at 70°C that has been subjected to 6 h additional drying at this temperature. The corresponding extinction spectra are shown in Figure 7.

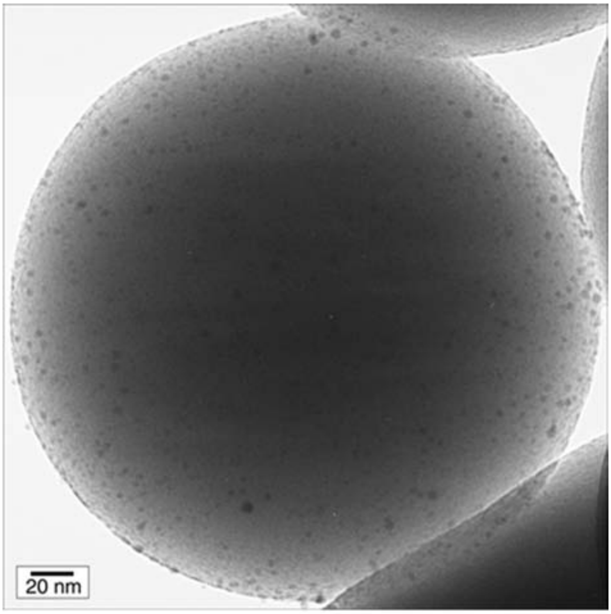

(a)

FIGURE 4 TEM image (a) and size distribution (b) of Au nanoparticle (1% precursor) on Stöber silica nanospheres (300 nm) upon drying 2 h at 70°C.

CONCLUSION

Summarizing the results of the metal coating experiments using incipient wetness impregnation one may conclude, that with both metals applied a uniform and reasonably dense nanoparticulate coverage of monodisperse silica nanospheres could be achieved. It is well suited to prepare metal nanoparticle coatings on monodisperse silica nanospheres without external reducing agents or media and absolutely free of adhesive aids or functionalizing agents usually applied to achieve particulate coatings. The general structure of particles of both metals is quite the same. Single crystalline particles of nearly cuboctahedral shape grow on the silica surface without indications of substrate-deposite interaction. With particle sizes increasing above about 5 nm, planar lattice defects and shape deviations occur indicating some changes in the growth mode. Despite the uniform arrangement of particles and relatively dense coverage of the oxide surface, the overall filling factor remains rather low. Consequently, the optical spectra mainly reflect the light scattering properties of silica nanospheres having a broad maximum at about 425 nm. Only upon higher metal loading, when

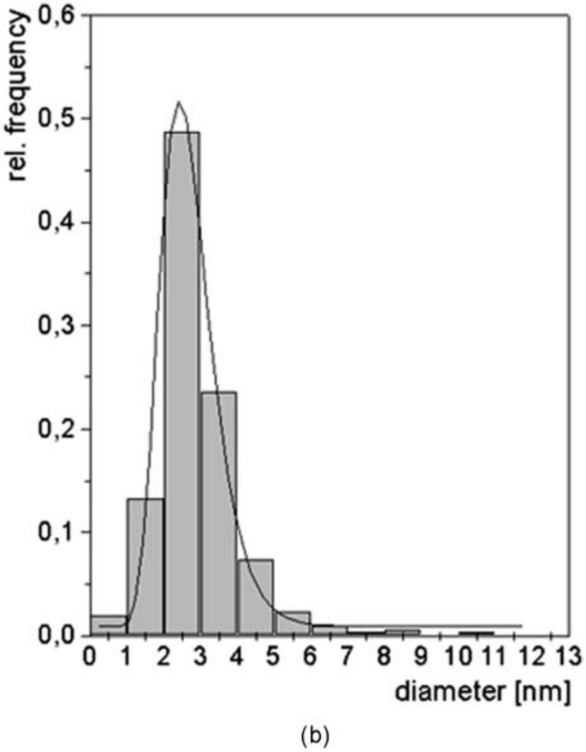

FIGURE 4 Continued.

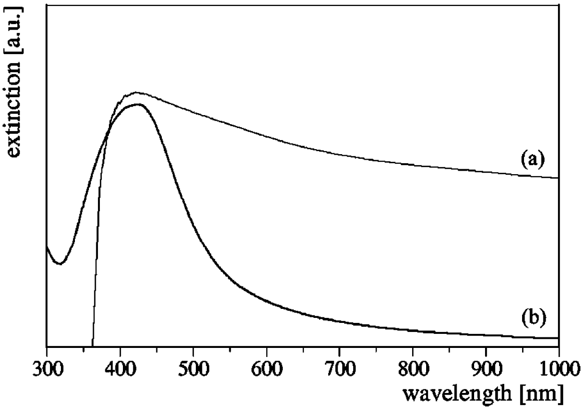

FIGURE 5 Extinction spectra of Ag nanoparticles coating Stöber silica (a) compared with the theoretical spectrum calculated using Mie theory (b).

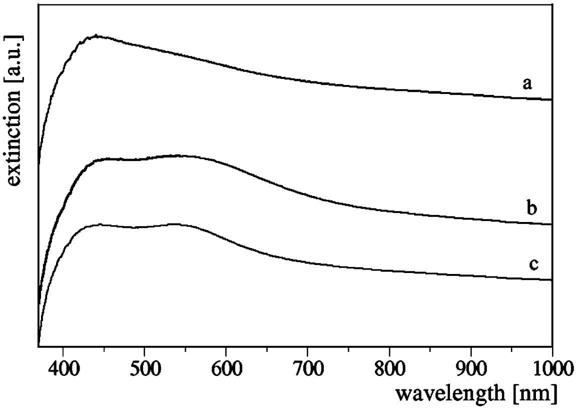

FIGURE 6 Extinction spectra of Au nanoparticles (1% precursor) upon drying at 120°C (a), 4 h additional drying at 200°C (b) and 2 h additional drying at 300°C (c).

resonance damping effects decrease because of increasing particle size, and particular for Au with the surface plasmon position at about 550 nm, the signature of metal particle resonances is observed. Core-shell resonances of the nanospheres studied are expected to occur not in the visible, but in the near infrared region, and only upon formation of closed shells. Although this aim was not yet attained, some improvements of the coating characteristics were achieved by variation of precursor concentration and drying temperature. Another way, repetition of the incipient wetness

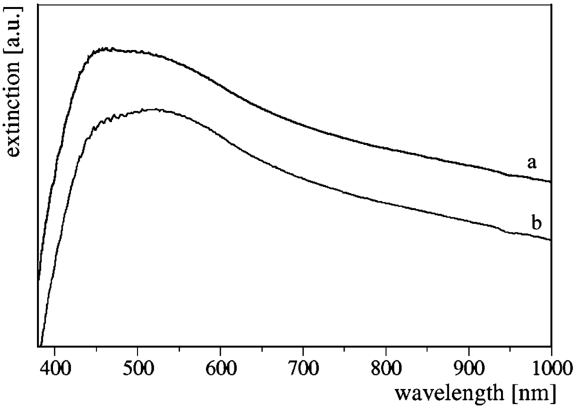

FIGURE 7 Extinction spectra of Au nanoparticles (1% precursor) upon drying at 70°C (a) and 6 h additional drying at 70°C (b).

impregnation and drying to compose a multi-step procedure, did not work well with Ag nanoparticles since the coverage did not increase accordingly, but a bimodal size distribution was produced. A similar procedure with Au, applying only half that concentration in the single step, produced a more satisfying result with a coverage increase distinctly above the one obtained by employing an equivalent concentration in a one-step procedure. It is important to note that from the observed behavior one cannot classify the multi-step procedure as a kind of seeding treatment. The accommodation of metal atoms, freshly formed in the second step, can occur on pre-existing particles, but in competition to nucleation processes on the not yet covered silica surface.

REFERENCES

[1] Kreibig, U. & Vollmer, M. (1995). *Optical Properties of Metal Clusters*, Springer Verlag: Berlin.
[2] Mie, G. (1908). *Ann. Phys. 25*, 377–445.
[3] Bohren, K. F. & Huffman, D. R. (1998). *Absorption and Scattering of Light by Small Particles*, John Willey and Sons, Inc.
[4] Maxwell-Garnet, J. C. (1904). *Philos. Trans. R. Soc.* London, *A203*, 385–420.
[5] Bruggeman, D. A. G. (1935). *Ann. Phys. (Leipzig)*, *24*, 636–679.
[6] Wiscombe, W. J. (1996). NCAR Thecnical Note, 1–64.
[7] Stöber, W., Fink, A., & Bohn, E. (1968). *J. Coll. Inter. Sci.*, *26*, 62–69.
[8] Sabia, R. & Ukrainczyk, L. (2000). *J. Non-Cryst Solids*, *277*, 1–9.